Circulation in the Eastern Levantine Basin Determined by Inverse Methods

ELI TZIPERMAN

Department of Earth, Atmospheric and Planetary Sciences, Massachusetts Institute of Technology, Cambridge, Massachusetts

ARTUR HECHT

Israeli Oceanographic and Limnological Research, Tel Shikmona, Haifa, Israel

(Manuscript received 21 April 1987, in final form 9 October 1987)

ABSTRACT

A finite difference linear inverse model is applied to hydrographic data from six summer and fall cruises in a small area (250 × 200 km) of the eastern Mediterranean sea. The temperature and salinity equations are used to form a linear set of equations for the reference geostrophic velocities and the mixing coefficients, which are then solved by singular value decomposition.

Advection by the horizontal velocities is the dominant process affecting the temperature and salinity fields in the region, and the model successfully resolves the horizontal velocities. Mixing and vertical advection are smaller by an order of magnitude, and the model cannot fully resolve the mixing coefficients and vertical velocities.

The six velocity fields calculated from the data indicate a very strong variability that makes it difficult to identify a repeating summer or fall circulation patterns on the scale of the region covered by the data.

An appendix contains the details of a new procedure for including linear inequalities in the solution of a rank deficient system of linear equations.

1. Introduction

The eastern Mediterranean Sea is an area of general interest to physical oceanography for several reasons. It is the source of the Levantine Intermediate water, (Wüst, 1960; Morcos, 1972; Özsoy et al., 1981), which is believed to be an important component of the high salinity Gibraltar outflow. Being reasonably accessible, the eastern Mediterranean can also be used to study water mass formation processes which are difficult to observe in polar formation regions.

Present knowledge of the region is mostly based on the analysis of historic hydrographic data (Wüst, 1960; El Gindy, 1982), but several recent observational programs provide new and interesting data from the region. The Israeli Oceanographic and Limnological Research Institute (IOLR) has been taking regular CTD measurements in a small region of the eastern Levantine Basin (Fig. 1) every 3–4 months for the last several years, forming a data base for the study of the region. An objective analysis of the data from one of the IOLR cruises which also included some XBT measurements was presented by Robinson et al. (1987). The recent observational program Physical Oceanography of the Eastern Mediterranean (POEM, 1985) is also expected to produce very useful basin-scale hydrographic data from this region.

In this paper several summer and fall cruises from the IOLR dataset are analyzed by inverse methods. Our main objective is to understand the physics of the region, in order to build a consistent inverse model for the eastern Mediterranean Sea. Because the area covered by the data is small, we are not able to calculate the general circulation. But with the excellent spatial and temporal coverage within the 200 km × 250 km measurements area, we are able to examine physical balances (importance of horizontal and vertical advection, mixing, etc.), and examine the temporal variability of the circulation. The experience gained here, in particular concerning the temporal variability, would be useful in critically examining time aliasing problems in the general circulation calculated from climatological hydrography or quasi synoptic basin scale POEM data.

This paper has two additional purposes: In the Appendix we present a new procedure for including linear inequalities in the SVD (singular value decomposition) solution of a rank deficient (underdetermined) linear system of equation. Finally, the IOLR data is unusual because it gives both time and space coverage of the region, and it can therefore be used to examine questions related to the calculation of the time-mean oceanic general circulation from hydrographic data. The work presented here serves as a basis for such a study (Tziperman, 1988).

Corresponding author address: Eli Tziperman, Isotope Research Department, Weizmann Institute of Science, Rehovot, 76100 Israel.

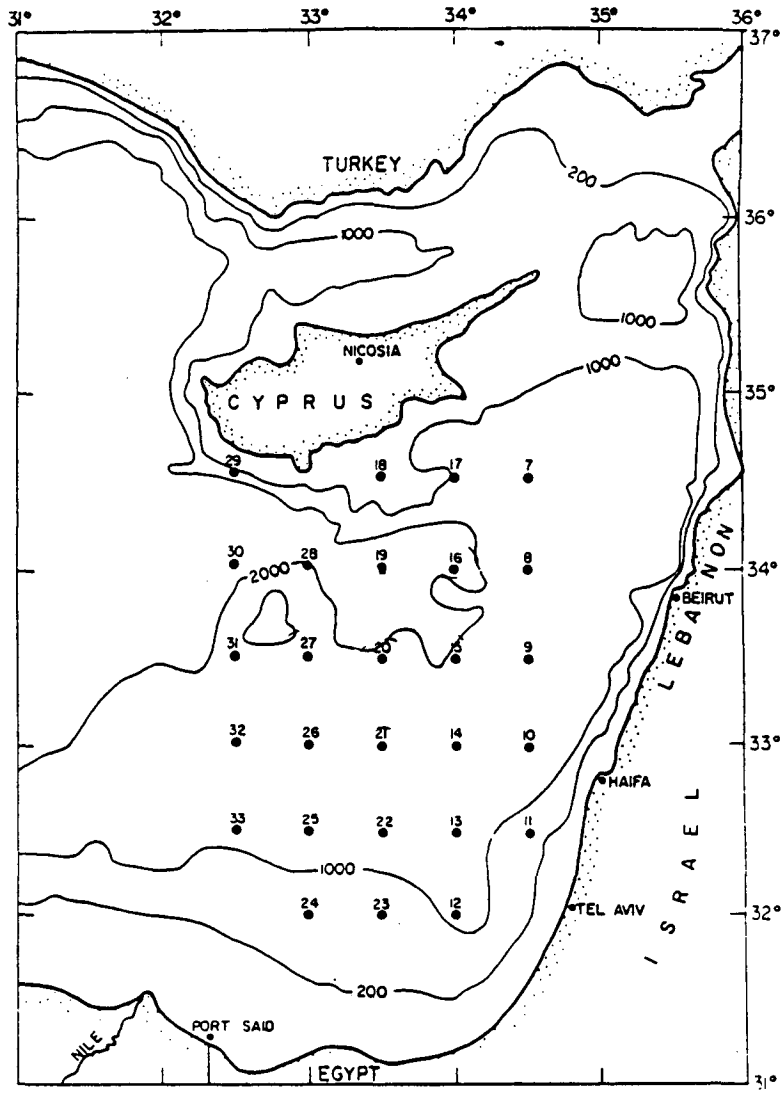

FIG. 1. Location of CTD stations taken in each of the cruises, and bottom topography of the region.

The following sections describe the dataset (2) and the development of the inverse model (3), present and discuss the inversion results for six summer cruises (4), and summarize the main conclusions (5).

2. The dataset and preliminary data treatment

The data used for the inverse calculation is part of an extensive dataset acquired by IOLR in the eastern Levantine Basin of the Mediterranean Sea from 1979 to 1984. The data were collected on 17 cruises, each about ten days long, separated by 3–4 months periods. During each cruise the 27 CTD stations shown in Fig. 1 were occupied. The stations were arranged in a 5 by 6 regular grid, with half-degree spacing in latitude and longitude. Initial quality control, bin averaging over 1 decibar intervals, and calculations of salinity, density, potential temperature etc. were all done at IOLR.

The inverse model presented below uses advection–diffusion equations for the temperature and salinity to calculate the absolute geostrophic velocity field. During the winter months, the water of the region is homogenized by strong mixing to a depth of two to three hundred meters. The simplified diffusion terms in the equations are probably not valid in the presence of very strong winter mixing and catastrophic sinking events. Therefore, only data from summer and fall seasons are used in the inverse calculation.

The summer water mass structure in the eastern Levantine basin is characterized by high surface salinity, a North Atlantic water salinity minimum at 50–100 m, and a salinity maximum at about 300 m mark-

ing the depth of the Levantine Intermediate water (Fig. 2). Cruises in which the characteristic temperature and salinity profiles were not fully developed due to a particularly severe preceding winter were discarded. After removing several additional cruises with possible data problems, six cruises were left, and were used in the inverse model: MC13 (July 1979), MC14 (August–September 1980), MC15 (November, 1980), MC18 (August, 1981), MC19 (November, 1981) and MC24 (October, 1983).

To prepare the data for the inverse calculation, the vertical coordinate was transformed from pressure to depth using the algorithm given by Saunders and Fofonoff (1976), profiles were smoothed by a 20 meter running average to remove small scale structure, and were subsampled in the vertical to obtain potential temperature, salinity and density at 30 standard depths specified by the model grid (see next section).

3. The inverse model

a. *Model equations*

The model equations are geostrophy, mass conservation, and steady state advection diffusion equations for the temperature and salinity fields

$$fu = -(1/\rho_0)p_y$$

$$fv = (1/\rho_0)p_x$$

$$p_z = -g\rho$$

$$u_x + v_y + w_z = 0$$

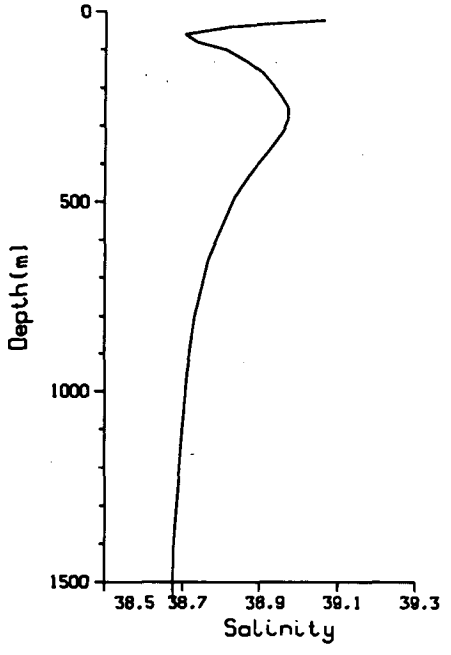

FIG. 2. (a, b) Average summer salinity profile for the eastern Levantine basin. (The average is over six summer cruises).

$$uT_x + vT_y + wT_z = [\kappa_v(z)T_z]_z + \kappa_H(z)\nabla_H{}^2T$$

$$uS_x + vS_y + wS_z = [\kappa_v(z)S_z]_z + \kappa_H(z)\nabla_H{}^2S. \quad (1)$$

Mixing of salt and heat is parameterized with horizontal and vertical eddy mixing coefficients which are possibly functions of depth. Because the area covered by the data is small (250 km by 200 km), it did not seem necessary to allow for horizontal variation of the mixing coefficients. In a stably stratified ocean, mixing along isopycnals by mesoscale eddies is much stronger than cross-isopycnal mixing due to small scale turbulence, salt fingers, etc. It is possible to use tensor diffusivities to parameterize the long and cross isopycnal mixing (Redi, 1982; Olbers et al., 1985). But as long as the isopycnal slope is not too large, vertical and horizontal mixing coefficients may be used to replace the cross- and long-isopycnal mixing coefficients without introducing large errors. As will be seen below, the mixing coefficients are, in any case, not very well resolved by the model. The uncertainty in their values due to resolution problems is probably much larger than errors due to the simplified parameterization used.

The time independent temperature and salinity equations used here probably hold to a good approximation deep enough below the surface water. The salinity of the surface water in the eastern Levantine basin increases during the summer due to the high local evaporation, and the surface circulation is affected by the time scales of the wind and buoyancy forcing (3–4 months, see May, 1982). But the high salinity values do not penetrate into the deep water until the convection and strong mixing of the winter season, and due to the slow baroclinic adjustment process, the deep circulation is expected to have longer time scales than those of the wind forcing. In the inversions shown below we have therefore used data only from below 160 m, where a steady state model is expected to be valid.

In accordance with the relatively small scales of the circulation in the region, a f-plane approximation to the geostrophic equations was used (the Coriolis parameter $f = f_0$ = constant). The horizontal geostrophic velocities are then nondivergent ($u_x + v_y = 0$) by (1a, b), and the vertical velocity is depth independent to lowest order ($w_z = 0$) by (1d). A nonzero constant vertical velocity is permitted although a more rigorous scaling (Pedlosky, 1979) may require the constant w to vanish. We prefer to let the inverse model determine the constant w most consistent with the tracer fields. The choice of a depth independent vertical velocity is further discussed below.

The f-plane approximation is also consistent with the results of numerical experiments for the eastern Mediterranean (Bergamasco and Malanotte-Rizzoli, 1986), showing the β effect not to be important in the dynamics of the region.

From the geostrophic and hydrostatic equations (1a, b, c), the thermal wind equations are obtained

$$fu_z = \frac{g}{\rho_0}\rho_y, \quad fv_z = -\frac{g}{\rho_0}\rho_x. \tag{2}$$

Integrating these equations in z, from a reference level, the vertical structure of the horizontal circulation is found in terms of the known density field. The full velocity field can be written as

$$u(x, y, z) = u_0(x, y) + \int_{z_0}^{z} \frac{g}{\rho_0 f_0}\rho_y dz',$$

$$v(x, y, z) = v_0(x, y) + \int_{z_0}^{z} \frac{-g}{\rho_0 f_0}\rho_x dz'$$

$$w(x, y, z) = w_0(x, y), \tag{3}$$

where $u_0(x, y) = u(x, y, z_0)$, v_0 and w_0 are the unknown velocities at the reference level.

Substituting the velocity field (3) in the advection diffusion equations for the temperature and salinity (1e, f),

$$u_0(x, y)T_x(x, y, z) + v_0(x, y)T_y(x, y, z) + w_0(x, y)T_z(x, y, z) - (\kappa_V(z)T_z)_z - \kappa_H(z)\nabla_H{}^2T = \Gamma(x, y, z), \tag{4}$$

where Γ represents the advection of temperature by the known relative velocities in (3). Evaluating T_x, T_y and T_z, as well as the geostrophic velocities relative to the reference level, in terms of the known temperature and density fields, and forming a similar equation for the salinity, we obtain linear equations for the unknown reference velocities and mixing coefficients. These equations can be formed at any depth where data is available, to obtain many equations for the problem's unknowns—reference velocities and mixing coefficients.

Derivatives in (4) were evaluated by center differences, using a grid following stations location in the horizontal, and with 30 vertical levels. Equation (4) was evaluated at all horizontal locations with data on all four sides (required for the center differences), and at ten levels. The mixing coefficients were expanded in Chebyshev polynomials

$$\kappa_V(z) = \sum_{n=0}^{N_V} C_{V,n}T_n(1 - 2z/D), \tag{5}$$

where D is a normalization constant making sure that the argument of T_n is in the range $(-1, 1)$, and was chosen to be the maximum depth of data for all stations. A similar expression holds for $\kappa_H(z)$, and the mixing coefficients are required to be positive at levels where equations are evaluated. Hogg (1987) used a similar expansion in Chebyshev polynomials to represent the horizontal structure of the mixing coefficients in the inverse. Equations (4) were written in matrix form $\mathbf{Ab} = \Gamma$, and the positivity condition was written as a set on linear inequalities for the Chebyshev coefficients $\mathbf{Gb} \geq 0$. The vector $\mathbf{b}$ contains the unknown reference velocities and Chebyshev coefficients, $\mathbf{A}$ and $\mathbf{G}$ are known matrices, and Γ is a column vector containing the rhs of (4). The number of equations, N, was typically about 200 [10 levels × 2 tracers (T, S) × 10 stations with four neighboring stations with data], while the number of unknowns was about 40 [10 stations × 3 reference velocities at each station, + about 10 Chebyshev coefficients from (5)]. The linear problem

$$\mathbf{Ab} = \Gamma, \quad \mathbf{Gb} \geq h \tag{6}$$

is solved by singular value decomposition (SVD) (Wunsch, 1978), using a modification of the LSI/LDP algorithm of Lawson and Hanson (1974) to include the inequalities. Details of incorporating the inequalities in the SVD solution are given in the Appendix.

The finite difference inverse model used here is very similar to the β-spiral inverse used by Olbers et al. (1985) (see also Schott and Stommel, 1978; and the finite difference inverse presented by Fiadeiro and Veronis, 1984).

b. Difficulties with calculating the vertical velocity

The profile of the vertical velocity can be calculated from the density field by integrating the vorticity equation (Olbers et al., 1985). This approach was tried, but the variable vertical velocity profile did not reduce the residuals, and the reference vertical velocities were not resolved by the model. As will be seen below, the model cannot resolve even the depth independent vertical velocity, so that there is no need to try and complicate the model by allowing vertical variations in w.

The inability of the model to resolve the vertical velocities can be explained by considering the magnitude of the different advection terms in the tracer equations. Let the horizontal and vertical scales of motion be L and H. Denote the scale of temperature variations along the horizontal and vertical scales of motion by $\Delta_H T$ and $\Delta_V T$ respectively, and the expected magnitude of the horizontal and vertical velocities by U and W respectively. The ratio of the horizontal and vertical advection terms in the temperature equation is then

$$\frac{wT_z}{uT_x} \approx \frac{WL}{UH}\frac{\Delta_V T}{\Delta_H T}. \tag{7}$$

Although one normally scales the vertical velocity w by UH/L, this is only an upper bound on its magnitude. For quasi geostrophic motions, with $\beta L/f = \mathrm{O(Ro)}$ (Ro = U/fL is the Rossby number, and $\beta = df/dy$), the magnitude of w is (Pedlosky, 1979) $w \sim W = (UH/L)\,\mathrm{Ro} \ll UH/L$. (Our f-plane model is simply the zero order approximation of a quasi geostrophic model, so we may use the above scaling for w.) Substituting the scales $U = 5$ cm s^{-1}, $L = 50$ km, $f = 7 \times 10^{-5}$ s^{-1}, and $\Delta_V T/\Delta_H T = 10$ (probably larger than needed), we find

$$\frac{wT_z}{uT_x} \approx \mathrm{Ro}\,\frac{\Delta_V T}{\Delta_H T} \approx \frac{1}{7}. \tag{8}$$

From (8) it is evident that the advection of temperature by the vertical velocity is much smaller than the advection by the horizontal velocities. The vertical advection is close to the order of magnitude of the noise in Eq. (4), and the inverse model cannot, therefore, resolve the vertical velocities.

A final comment concerning the vertical velocity: in the presence of strong bottom topography (Fig. 1), one may expect the vertical velocity induced at the bottom to be non negligible. In practice, however, the inverse cannot resolve the vertical velocity, so we are consistent in assuming that it is small. It is possible, in principle, to deduce w at the top from wind curl data, or from the bottom boundary condition. But this requires w vary with depth (because the values of w found from the top and bottom boundary conditions may be different), while we ignore the vertical structure of w.

c. *SVD solution*

1) Weighting

Before calculating the SVD of $\mathbf{A}$ and solving (6) for $\mathbf{b}$, one normally weights the equations and unknowns (Wiggins, 1972; Wunsch, 1978). The weighted problem can be written as

$$(\mathbf{S}^{-1/2}\mathbf{A}\mathbf{W}^{1/2})(\mathbf{W}^{-1/2}\mathbf{b}) = \mathbf{S}^{-1/2}\Gamma \pm \mathbf{S}^{-1/2}\epsilon. \tag{9}$$

In general $\mathbf{W}$ and $\mathbf{S}$ are the covariance matrices of the unknowns $\mathbf{b}$ and the noise in each equation ϵ. Having no a priori information about the noise correlation, and no reason to specify a priori correlation between the unknowns, diagonal weighting matrices are used.

Errors in the Eqs. (6) for the reference velocities and mixing coefficients are in part due to measurement errors, but mostly due to unresolved small scale processes like internal waves. With no information about the magnitudes of these errors [ϵ in (9)], the rows of $\mathbf{A}$ were normalized by their length, so that all equations are treated equally in the inversion

$$\mathbf{S}_{ii}^{1/2} = \Big(\sum_{j=1}^{M} a_{ij}^2\Big)^{1/2}. \tag{10}$$

The column weights, $W^{1/2}$, are given by (Wunsch, 1978)

$$W_{jj}^{1/2} = [b_j]^{1/2}\Big(\sum_{i=1}^{N} a_{ij}^2\Big)^{-1/4} \tag{11}$$

where a_{ij} are the elements of the matrix $\mathbf{A}$; N, M are the number of equations and unknowns respectively, and $[b_j]$ is the expected magnitude of the jth unknown in $\mathbf{b}$.

2) Choosing the rank of A

Although there are always more equations than unknowns in the present model ($N > M$), the equations matrix $\mathbf{A}$ is never full rank. To determine the rank of $\mathbf{A}$ a criterion of maximum allowed variance (Wiggins, 1972) was used, because it permits direct control over the amount of noise in the solution. The rank (k) of $\mathbf{A}$, was typically about 25 to 30.

The rank was always such that the horizontal reference velocities were resolved (diagonal elements of the parameter resolution matrix about 0.99), vertical reference velocities were not resolved, and mixing coefficients were partly resolved (diagonal elements of parameter resolution matrix about 0.3), (see Wunsch, 1978, or Wiggins, 1972, for a detailed discussion of the resolution matrices).

3) Residuals: Is the model consistent with the data?

Let $\hat{u}$, $\hat{\kappa}_V$ and $\hat{\kappa}_H$ be the total velocity field and mixing coefficients calculated by the inverse. With more equations than unknowns, there are always residuals

$$\hat{u}\cdot\nabla T - (\hat{\kappa}_V(z)T_z)_z - \hat{\kappa}_H(z)\nabla_H^2 T = r(x, y, z) \neq 0. \tag{12}$$

The residuals $r(x, y, z)$ may be viewed as a time change term in the temperature equation, due to the inability of the model to satisfy the steady state advection diffusion equation: $r \sim \partial T/\partial t$. Multiplying $r(x, y, z)$ by 3 months, gives an equivalent temperature change expected to occur at (x, y, z) within a 3-month period, due to the residuals. Comparing this equivalent temperature change to the natural variability around steady state, which occurs at (x, y, z), one can decide whether the model adequately describes the data. As an estimate for the natural variability, we calculate the rms of the temperature and salinity fields, using the data from the six summer cruises.

4) Error estimates

The SVD estimate for the covariance of the parameter vector $\mathbf{b}$ is made of two parts: one due to errors in the data, and the second due to lack of resolution of the parameters (Wiggins, 1972). The error bars shown in the profiles for the mixing coefficients represent only the first part of the error estimate—for the noise variance only. Because the mixing coefficients are resolved only to about 30%, the shown error bars should be multiplied by about three to obtain the order of magnitude of the full error bars for the mixing coefficients.

d. *Calibrating the model*

In order to decide on the final details of the model to be applied to the data from the six cruises, we have tried several versions of the model on the data from a single cruise (MC24). These experiments are summarized here, and were described in detail in Tziperman (1987).

Using the tracer equations without mixing to calculate the reference velocities reduced the residuals [see (12)] by about 50% compared to those found when specifying a level of no motion (at 460 m). The addition of vertical mixing to the tracer equations did not cause significant additional reduction in the residuals, but did eliminate some non random structure from the residuals found in the model without mixing for the deep levels.

The mixing coefficients were resolved only to about 30%, and their magnitude was around several $cm^2\ s^{-1}$. Up-weighting the vertical mixing coefficient in the inversion by specifying a priori value of 10 instead of 1 $cm^2\ s^{-1}$ [see (11)] improved its resolution to about 40%, but did not change the magnitude of the solution for the coefficient. This result indicates that the magnitude of the mixing coefficients is not likely to be larger than what was found here.

Adding the horizontal mixing did not improve the results significantly, and the horizontal mixing coefficients were also not very well resolved. Because one tends to trust vertical derivatives of the high vertical resolution CTD data more than horizontal derivatives taken from the data, it was decided to include only the vertical mixing in the model. A 10th-degree polynomial (5) was chosen to represent the depth dependence of the mixing coefficient. This allows a vertical resolution of the coefficients of about 300 m, about the height of the intermediate salinity maximum.

Figure 3 shows the different terms in the temperature equation as function of depth for one of the stations where Eq. (4) was evaluated. The dominant balance is between the horizontal advection terms, which take care of most of the residuals, with vertical advection and mixing an order of magnitude smaller.

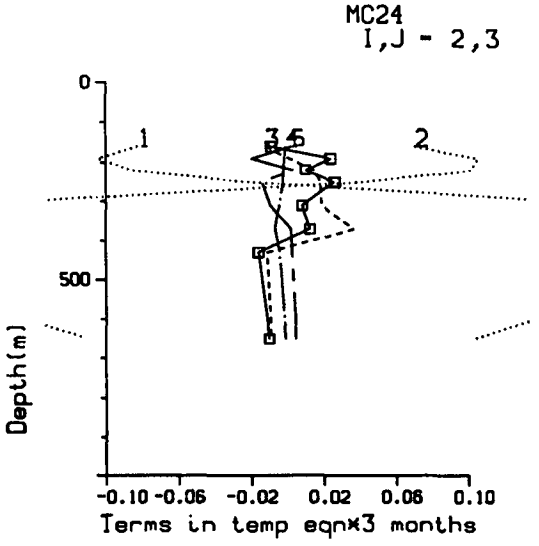

FIG. 3. Different terms in the advection–diffusion equations for the temperature. Dotted lines are the horizontal advection terms, uT_x, vT_y; the dashed line is the sum of the horizontal advection terms, $uT_x + vT_y$; the chain-dotted line is the vertical advection term wT_z and the chain-dashed line is the vertical diffusion term $[\kappa_v(z)T_z]_z$.

The well resolved horizontal velocities, were not sensitive to the initial reference level chosen, nor to the parameterization of the mixing used. We therefore conclude that the results—in particular for the horizontal velocity field—are believable, and proceed to use the final inverse model chosen here to analyze the data from all the six summer cruises. The initial reference level for the calculation was chosen as the deepest level in which data is available at all horizontal stations: 400 m for MC14, MC19 and 460 m for the rest of the cruises. (At some of the stations data were available below the reference level, and were used to evaluate equations at the deeper levels.)

4. Results for the six summer cruises

Figure (4) shows velocity vectors for the absolute flow field calculated by the inverse at three levels and for all six cruises. The profiles of the mixing coefficients calculated for the six cruises are shown in Fig. (5).

The variability of the region's circulation is very strong. Both the magnitude of the velocities and the structure of the circulation differ significantly from one cruise to another. The velocity calculated for different summer and fall cruises varies from 1–2 cm s^{-1} in MC24, to 10 cm s^{-1} in MC13 and MC19, and it is difficult to identify common features marking the summer or fall circulation of the region.

With the strong variability dominating the mean flows, one must be careful when calculating the circulation of the region—even for a given season—using data from an occasional cruise in the region. It is possible, though, that by using a smoothed climatological dataset with basin scale coverage, one would be able to identify more steady circulation patterns. Examining the velocity vector diagrams in Fig. 4, one can recognize features with horizontal scales of 100–150 km (for example, see the cyclonic gyre at 460 m and the anticyclonic gyres at 208 and 160 m, in MC15). It is possible, of course, that there is smaller and larger scale variability not resolved by the data.

In many of the cruises there is an increase in the velocity from the depth of the Levantine Intermediate Water (LIW), to the deeper level shown (Fig. 4) at 460 m. There is a corresponding zero crossing of the horizontal advection terms around the level of the LIW in many stations (profiles 1 and 2 in Fig. 3). The strong salinity and temperature signal at the LIW level seems to create large horizontal gradients, and the inverse is forced to reduce the velocities at this depth (by increasing it at the initial reference level at 460 m), in order to reduce the residuals at the depth of the LIW. If we suppress this minimum by down weighting the equations at the LIW level, the dimensional residuals there

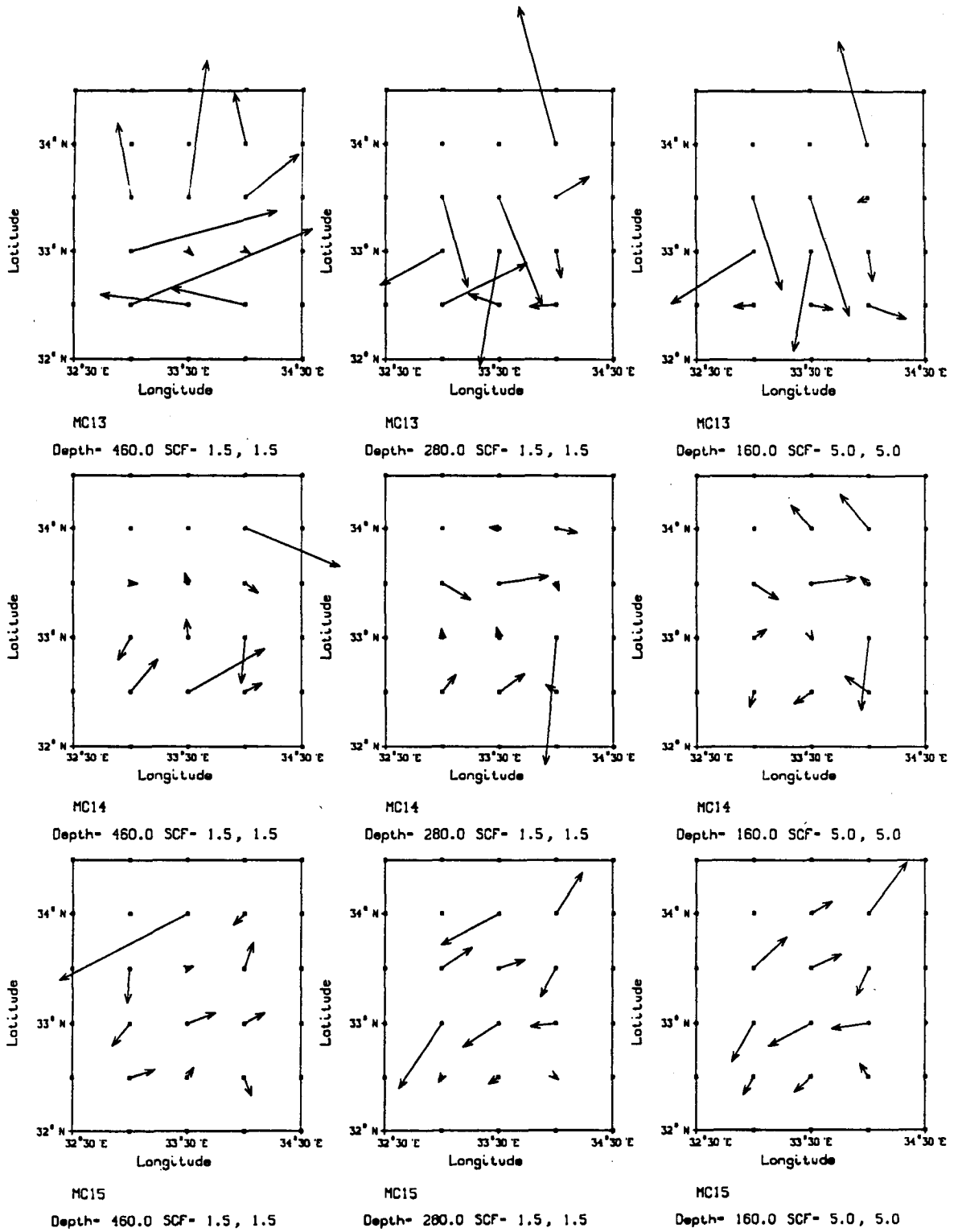

FIG. 4. Velocity vectors for the six cruises at three levels. The distance between tick marks on the axes is equivalent 5 cm s^{-1} for the upper level and 1.5 cm s^{-1} for the lower two levels.

rise above the level of natural variability (i.e., noise level), indicating inconsistent solution. This suggests that the velocity minimum is real and not a result of the weighting used here. Direct current measurements are necessary to satisfactorily resolve this issue.

The mixing coefficients calculated for the six cruises

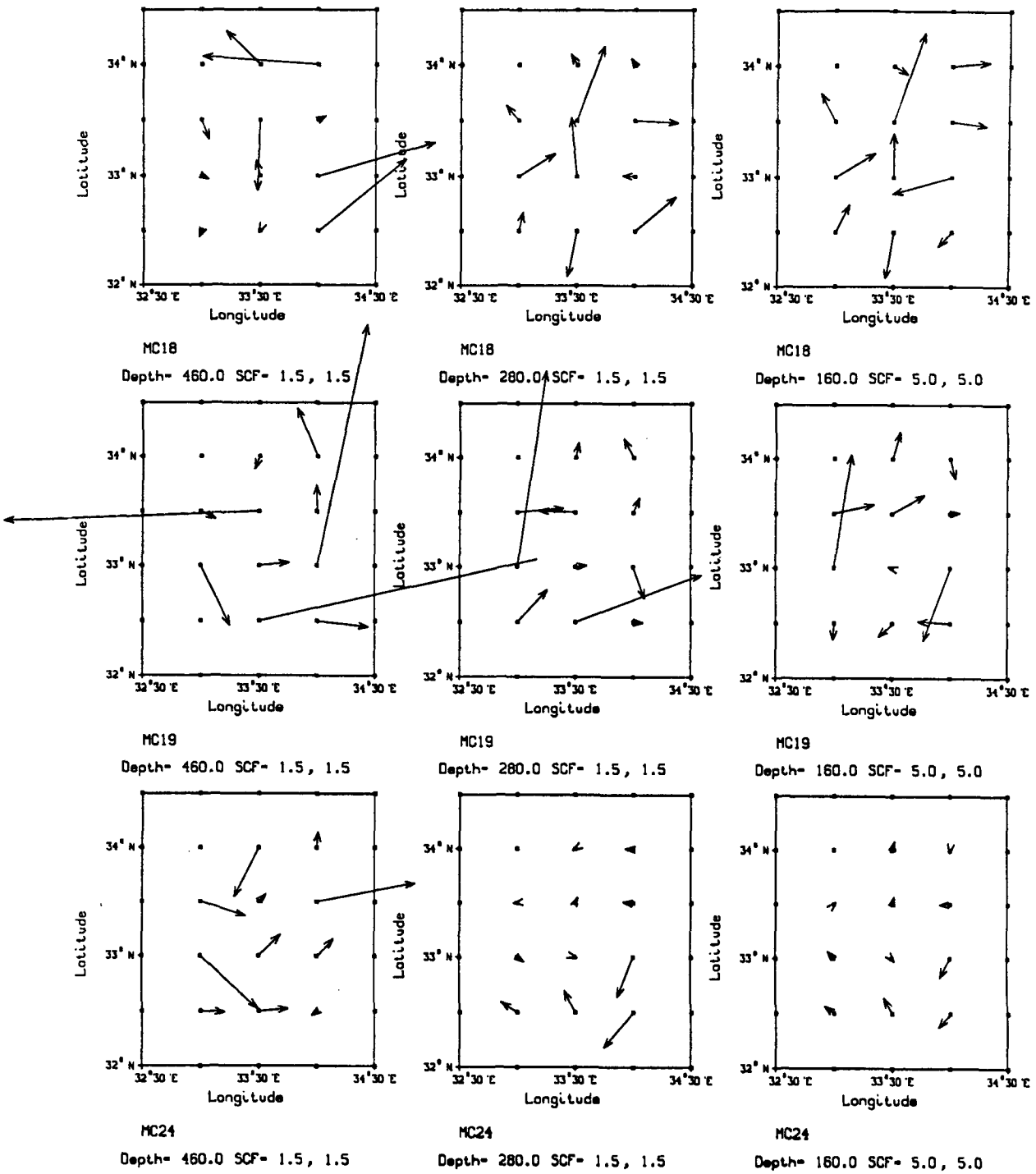

FIG. 4. (*Continued*)

(Fig. 5) are not significantly different from zero when the error due to the lack of resolution is included. The mixing terms were not crucial to the success of the model in reducing the residuals.

The residuals found for most of the cruises are acceptable according to the criteria described in the previous sections. There are problems, however, with the more energetic cruises, MC13 and MC19. The residuals of the temperature and salinity equations evaluated at some locations were larger than may be expected due to errors in the data and the natural variability around the mean summer fields. The reason for that may be

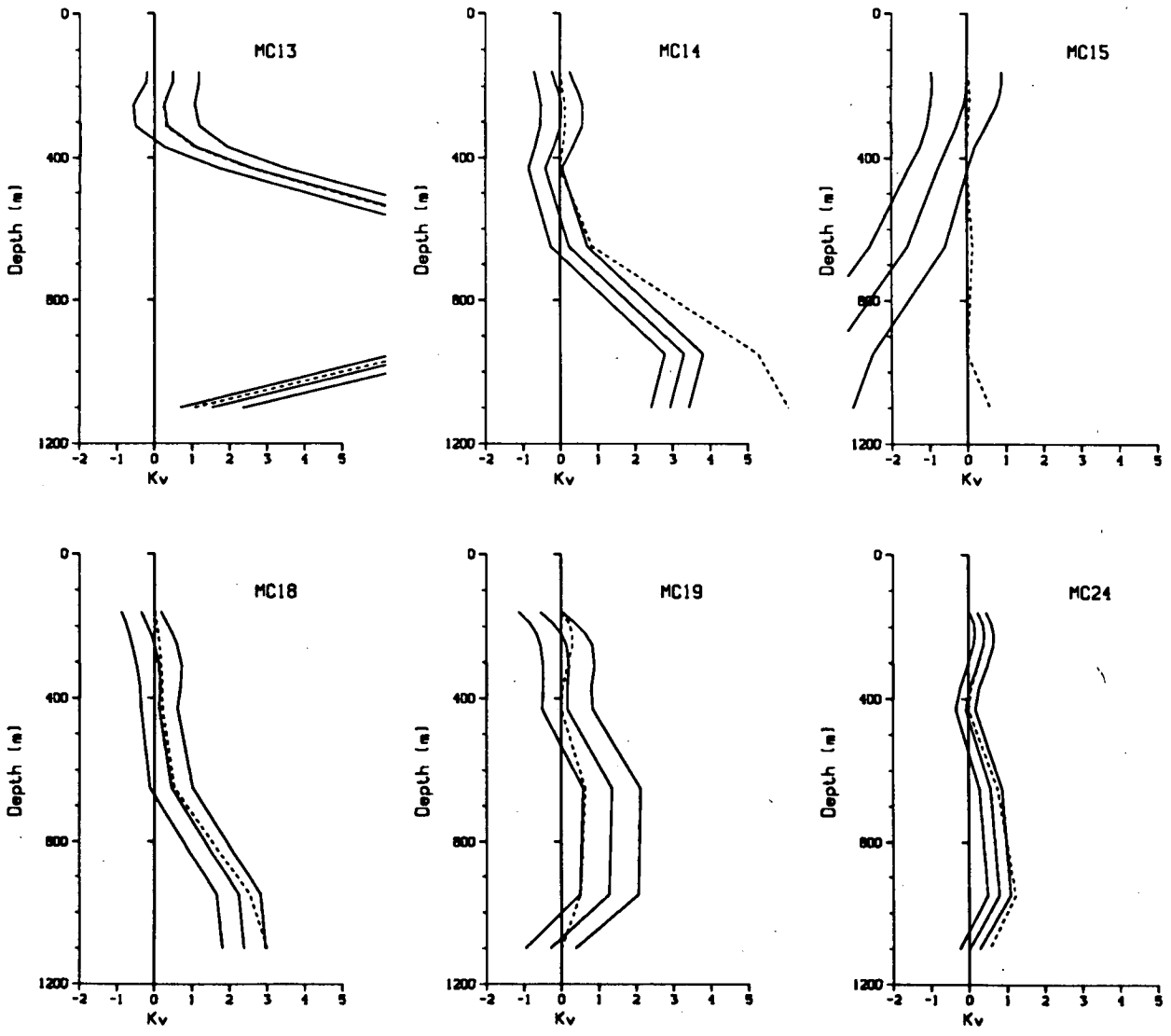

FIG. 5. Profiles of the vertical mixing coefficients calculated for all of the six cruises. The three solid lines are the SVD solution and error bars, and the dashed line is the value of the mixing coefficients when inequalities forcing it to be positive are applied. Units are $cm^2\ s^{-1}$.

the aliasing of the data by the small but strong mesoscale eddies in the region. Time variations and nonlinear vorticity balance which may be important for the small eddies but are not included in the model, may have caused the increase in residuals.

Figure 6 compares the residuals and circulation found by the inverse when using the data with only limited vertical averaging done (see §2), and when using objective mapping (Bretherton et al., 1976) with a 150 km correlation distance to filter out the eddies. The residuals are smaller and more acceptable for the smoothed data. The circulation calculated from the smoothed data is similar to that obtained from the non smoothed data, although weaker.

In spite of the somewhat larger residuals in two of the cruises, it seemed preferable to present the inverse results obtained from the "raw" data rather than the smoothed one. The smoothed data probably does not represent the time mean fields, or even the mean seasonal fields, as the different smoothed summer cruises are not similar. We believe that the circulation presented in Fig. 4 is a better representation of the actual circulation of the region during the six cruises than that calculated from the smoothed data. Smoothing by objective mapping may still be necessary when calculating the basin scale circulation of the region from climatological data, to filter out the strong mesoscale eddies.

5. Discussion and summary

A finite difference inverse model was applied to hydrographic data collected in six summer and fall cruises in the eastern Levantine Basin of the Mediterranean

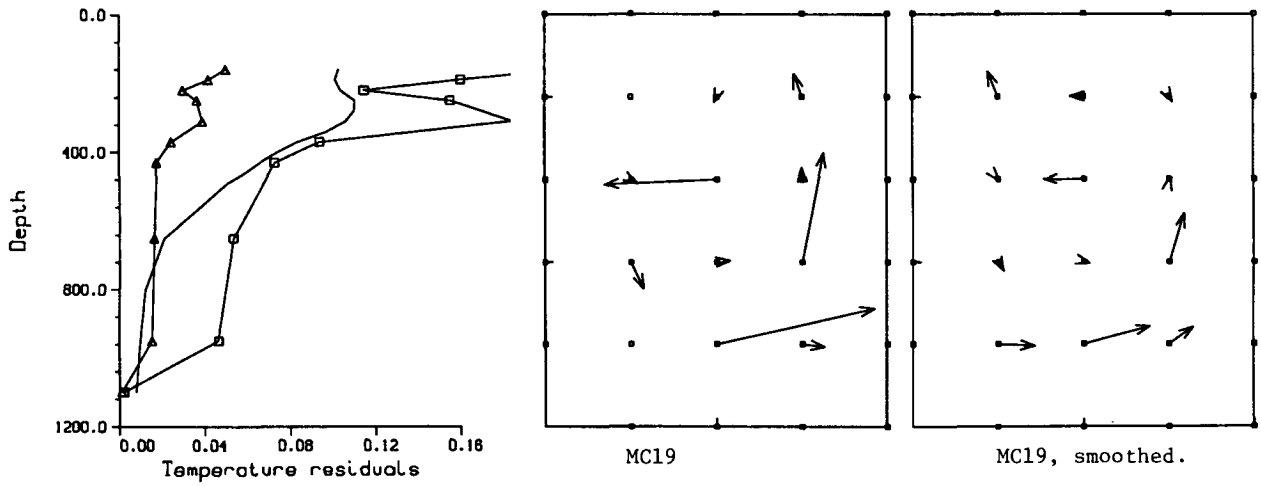

FIG. 6. Comparing the circulation at 460 m and horizontally averaged residuals $\int\int |r(x, y, z)|\,dxdy$ when using the raw and smoothed data. The profiles show the residuals obtained from the non smoothed and smoothed data (squares and triangles respectively), together with the rms of the region's temperature profile, indicating the natural variability of the region, and calculated from data of the six cruises. Residuals are multiplied by 3 months, and shown in degrees Celsius. Scale for the velocity vectors is as in Fig. 4.

Sea. The model consists of the geostrophic equations, mass conservation, and advection diffusion equations for the temperature and salinity. Mixing processes are parameterized with vertical eddy mixing coefficients, and the vertical velocity is taken to be depth independent. The model is used to calculate absolute geostrophic velocities and mixing coefficients.

The model successfully explains the temperature and salinity fields in the eastern Levantine region, with residuals in the advection diffusion equations below the noise level due to natural variability in the region. Smoothing of the hydrography by objective mapping was necessary to obtain acceptable residuals for the more energetic cruises. When calculating the circulation of the entire Levantine basin, one probably ought to use such smoothing in order to filter out the strong mesoscale eddies.

Advection by the horizontal velocities is the dominant physical process affecting the temperature and salinity distributions, with mixing and vertical advection smaller by an order of magnitude. The model successfully resolves the horizontal velocities, but is unable to fully resolve the mixing coefficients and vertical velocities.

The circulation patterns and strength vary significantly from cruise to cruise, even for cruises that were taken at the same season. The variability is on scales of 100–150 km, much larger than the Rossby radius of deformation (15 km). Further studies are needed to connect the strong variability found to the forcing by wind, evaporation and bottom topography.

Because of the small size of the region covered by the data, it was impossible to infer the general circulation of the region. The results do show, however, that one has to be very careful when inferring the region's circulation from a single realization of the hydrography, as the results will be dominated by the very strong time dependent eddies.

Work is in progress to apply the knowledge and experience obtained in this study to the analysis of climatological hydrographic data, to calculate the basin-scale circulation of the eastern Mediterranean.

Acknowledgments. We want to thank Carl Wunsch for many useful suggestions and many careful readings of preliminary versions of this work. Discussions with Ichiro Fukumori on inequalities in SVD, with Haim Nelken on the finite difference formulation, as well as Charmaine King's help with the programming are gratefully acknowledged.

We are greatly indebted to the crew of the RV *Shikmona* and their skippers A. Zur and A. Ben-Num, to the scientists of the IOLR physical oceanography department J. Bishop, N. Z. Rosentraub; and to our technical staff G. Brookman, J. Mouwes, R. Sela and M. Udel whose hard work, support and patience made our endeavors feasible.

This work was done while Eli Tziperman was a student in the Woods Hole Oceanographic Institution/ Massachusetts Institute of Technology Joint Program in Oceanography, and supported by NSF Grants OCE-8521685 and OCE-8017791.

APPENDIX

Inclusion of Inequalities in the SVD Solution

Lawson and Hanson (1974, p. 168) gave an algorithm (LSI/LDP, which stands for least squares with inequality constraints, and least distance programming) for incorporating linear inequalities in the SVD solution of a linear system of equations. Given an equations matrix $\mathbf{A}_{n\times m}$ of rank m, a right hand side $\Gamma_{n\times 1}$, in-

equalities matrix and rhs $\mathbf{G}_{n_1 \times m}$ and $\mathbf{h}_{n_1 \times 1}$, the algorithm finds the vector solution $\mathbf{b}$ which minimizes $\|\mathbf{Ab} - \Gamma\|^2$ subject to $\mathbf{Gb} \geq \mathbf{h}$. The algorithm may not find the solution when the equations matrix $\mathbf{A}$ is not full rank, as happens in the model presented above. This appendix presents an extension of the LSI/LDP algorithm, to allow for rank deficient $\mathbf{A}$ matrices.

Fu (1981) incorporated inequalities in the SVD solution of an underdetermined system by looking for the smallest vector from the null space of the equations matrix $\mathbf{A}$ that will satisfy the inequalities. This method can satisfy only the null space part of the inequalities, and it may give an unphysically large solution when the null space is too small (i.e., when the problem is not very underdetermined). These problems are demonstrated below by a simple example. A different approach was taken by Olbers et al. (1985) who used a tapered cutoff modification to the LSI/LDP algorithm to eliminate the effects of very small eigenvalues on the parameter variance. The advantages and disadvantages of tapered cutoff versus sharp cutoff were discussed in detail by Wiggins (1972).

1. Example

Before going into the details of the mathematical formalism, consider the following simple example (shown in Fig. A1) demonstrating the difference between the approach here and in Fu (1981), and the difficulties with LSI/LDP when the system of equations is not full rank. The problem consists of a single equation (the line in Fig. A1), and one inequality (shaded region in Fig. A1). Fu's approach here is to find the SVD solution to the equation (dashed arrow in Fig. A1) and then to look for the smallest null space vector which brings the solution into the feasible space determined by the inequalities (shaded area in Fig. A1). The null space vector in this example lies along the line (a'–b), and therefore the smallest null space vector to bring the solution into the feasible space is (a'–b), and the solution is at (b). Note that the solution obtained this way has a large amplitude (0–b), which, in some cases may be nonphysical. In practical problems, the eigenvalues corresponding to the null space vectors are very small, but not necessarily zero. (One may want to term this the physical null space, to distinguish it from the mathematical null space containing strictly zero eigenvalues). Adding a large null space vector to the solution may therefore cause significantly larger residuals. (Adding null space vectors to the solution does not increase the residuals only when the corresponding eign values are identically zero.)

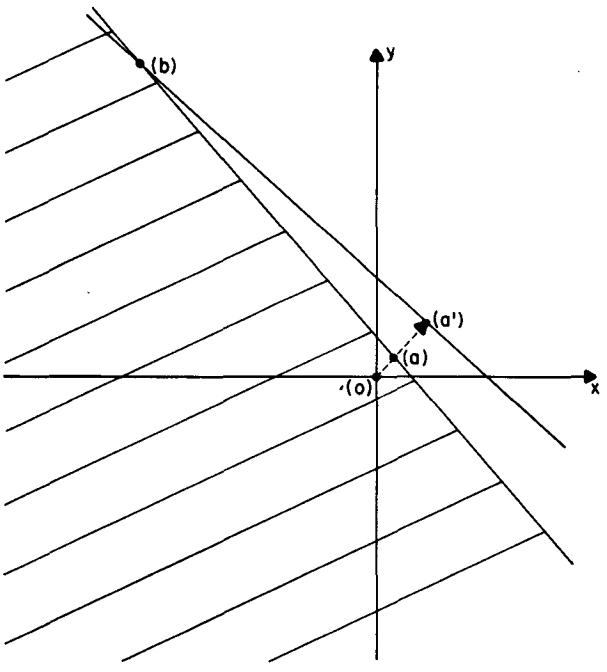

FIG. A1. Trying to solve non full rank system with LSI/LDP, Fu's method, and using the present approach. See text for details.

This is typically what happens in the model when we try to satisfy the inequalities on the mixing coefficients with the null space vectors only: the vertical velocities and the coefficients in the Chebyshev expansion of the mixing coefficients become unphysically large, and so do the residuals.

Finally, note that if the equation line (a'–b) is parallel to the feasible space (shaded region in Fig. A1) one cannot find a null space vector to satisfy the inequalities. More generally, the method is not able to satisfy the inequalities when one of the rows of $\mathbf{G}$ belongs to the range part of $\mathbf{A}$.

The LSI/LDP algorithm would try to minimize $\|\mathbf{Ab} - \Gamma\|^2$ subject to the inequalities. Because the system is not full rank, the algorithm searches for a solution only in the direction of the range vectors (i.e., in the direction of the SVD solution). The solution must therefore lie along in the dashed arrow in Fig. A1 in the feasible space, and as close as possible to the line (a'–b). The solution is then the point (a). Note that if the equation line is perpendicular to the feasible space, the LSI/LDP algorithm cannot find a solution, even if the inequalities are compatible. More generally, the algorithm cannot find a solution when the inequalities matrix is perpendicular to the range vectors of $\mathbf{A}$.

To make sure the solution can be found even when $\mathbf{A}$ is not full rank, without limiting the structure of the inequalities matrix $\mathbf{G}$, we need to allow searching for a feasible solution in any direction—range or null. The procedure outlined below searches for the solution that lies in the feasible space defined by the inequalities and requires the solution to have the smallest possible null space vector in addition to minimizing the residuals of the equations. The solution for the above example must lie then on the line (a–b), and the exact location depends on the relative weight given to minimizing the null space vector vs minimizing the residuals (see the parameter ϵ below). In general, if the inequalities are compatible, the algorithm outlined below will always

find a solution. If both Fu's and LSI/LDP solutions exists, the solution will lie somewhere between them.

2. The formalism

Given a system of equations $\mathbf{Ab} = \Gamma$, and inequalities $\mathbf{Gb} \geqslant \mathbf{h}$, where $\mathbf{A}$ is an $n \times m$ matrix of rank k, Γ is an $n \times 1$ column vector, $\mathbf{G}$ is as $n_1 \times m$ matrix, and $\mathbf{h}$ an $n_1 \times 1$ column vector, the SVD of $\mathbf{A}$ is

$$\mathbf{A} = \mathbf{U}_{n\times k}\Lambda_{k\times k}\mathbf{V}^{\mathrm{T}}_{k\times m}. \tag{1}$$

The solution to the system of equations, without the inequalities, may be written (Wunsch, 1978) as

$$\mathbf{b} = \mathbf{b}_{\mathrm{SVD}} + \mathbf{b}_{\mathrm{null}} = \sum_{i=1}^{k} \alpha_i \mathbf{V}_i + \sum_{j=k+1}^{m} \beta_j \mathbf{V}_j. \tag{2}$$

The first k $\mathbf{V}$ vectors are the columns of the $\mathbf{V}$ matrix from the SVD of the equations matrix $\mathbf{A}$. The other $m-k$ are orthonormal vectors spanning the null space part of $\mathbf{A}$. Fu (1981) described a way of calculating these null space $\mathbf{V}$ vectors.

We look for the solution vector $\mathbf{b}$ which solves the problem

$$\min\|(\mathbf{U}_{n\times k}\Lambda_{k\times k}\mathbf{V}^{\mathrm{T}}_{k\times m})\mathbf{b} - \Gamma\|^2 + \epsilon^2\|\mathbf{b}_{\mathrm{null}}\|^2,$$
$$\text{subject to} \quad \mathbf{Gb} \geqslant \mathbf{h}. \tag{3}$$

The small constant ϵ is discussed below. The solution to this problem is unique, because both the range and the null parts of b are constrained by the minimization. This is not the case when using LSI/LDP with a singular matrix $\mathbf{A}$, as demonstrated by the example above. It is important to note that only the range part of the matrix $\mathbf{A}$ (the first k eigenvalues) is taken into account when the algorithm given below minimizes $\|\mathbf{Ab} - \Gamma\|^2$ in (3). The solution to problem (3) is now found by transforming it to an equivalent LSI/LDP problem, and then using the Lawson and Hanson algorithm to solve it.

Let us now append $m - k$ equations to $\mathbf{A}$, and form a modified set of equations

$$\hat{\mathbf{A}}_{(n+m-k)\times m}\mathbf{b} = \begin{pmatrix} \mathbf{A}_{n\times m} \\ \epsilon\mathbf{V}^{\mathrm{T}}_{(m-k)\times m} \end{pmatrix}\mathbf{b} = \begin{pmatrix} \Gamma_{n\times 1} \\ 0_{(m-k)\times 1} \end{pmatrix} = \hat{\Gamma}. \tag{4}$$

The rows of the matrix $\mathbf{V}^{\mathrm{T}}_{(m-k)\times m}$ are the null space $\mathbf{V}$ vectors. The rank of this matrix is $m - k$, and because its rows are orthogonal to those of $\mathbf{A}$, the rank of the modified equation matrix, $\hat{\mathbf{A}}$, is $k + (m - k) = m$.

The LSI/LDP algorithm may now be used to solve the modified problem, with the full rank $\hat{\mathbf{A}}$. The LSI/LDP problem is now

$$\min\|\hat{\mathbf{A}}\mathbf{b} - \hat{\Gamma}\|^2, \quad \text{subject to} \quad \mathbf{Gb} \geqslant \mathbf{h}. \tag{5}$$

But

$$\begin{aligned} \|\hat{\mathbf{A}}\mathbf{b} - \hat{\Gamma}\|^2 &= \left\| \begin{pmatrix} \mathbf{A}_{n\times m} \\ \epsilon\mathbf{V}^{\mathrm{T}}_{(m-k)\times m} \end{pmatrix}\mathbf{b} - \begin{pmatrix} \Gamma_{n\times 1} \\ 0_{(m-k)\times 1} \end{pmatrix} \right\|^2 \\ &= \|\mathbf{Ab} - \Gamma\|^2 + \epsilon^2\|\mathbf{V}^{\mathrm{T}}_{(m-k)\times m}\mathbf{b}\|^2 \\ &= \|\mathbf{Ab} - \Gamma\|^2 + \epsilon^2\|\mathbf{b}_{\mathrm{null}}\|^2 \end{aligned} \tag{6}$$

so that the modified problem (5) with the full rank equations matrix $\hat{\mathbf{A}}$ is equivalent to the problem (3) which we want to solve.

The LSI/LDP algorithm requires the SVD of the $\hat{\mathbf{A}}$ matrix to be known. This can be written in terms of the already known SVD of the smaller original equations matrix $\mathbf{A}_{n\times m}$, and there is no need to recalculate the SVD for the larger matrix. Defining

$$\begin{aligned} \hat{\mathbf{U}}_{(n+m-k)\times m} &= \begin{pmatrix} \mathbf{U}_{n\times k} & 0_{n\times(m-k)} \\ 0_{(m-k)\times k} & \mathbf{I}_{(m-k)\times(m-k)} \end{pmatrix}, \\ \hat{\Lambda}_{m\times m} &= \begin{pmatrix} \Lambda_{k\times k} & 0_{(m-k)\times(m-k)} \\ 0_{(m-k)\times(m-k)} & \epsilon\mathbf{I}_{(m-k)\times(m-k)} \end{pmatrix}, \\ \hat{\mathbf{V}}_{m\times m} &= \begin{pmatrix} \mathbf{V}_{k\times m} \\ \mathbf{V}_{(m-k)\times m} \end{pmatrix}, \end{aligned} \tag{7}$$

it is not difficult to see that

$$\hat{\mathbf{A}} = \hat{\mathbf{U}}\hat{\Lambda}\hat{\mathbf{V}}^{\mathrm{T}}.$$

3. Choosing ϵ

Consider again Fig. A1, to see the effect of varying the magnitude of ϵ. The example is of two unknowns, one equation (the line a'–b), and one inequality (shaded area). The solution to problem (3) in this case must lie on the line a–b, in the feasible space, but its exact location is determined by ϵ. When ϵ is very small, minimizing $\|\mathbf{Ab} - \Gamma\|^2 + \epsilon^2\|\mathbf{b}_{\mathrm{null}}\|^2$ is equivalent to minimizing $\|\mathbf{Ab} - \Gamma\|^2$ only. There is a weak constraint only on the size of the null space vector, and the solution approaches the point b. If, on the other hand, ϵ is chosen larger, then the algorithm tries to minimize the null space vector while staying in the feasible space, and the solution moves towards the point a.

Two considerations which may help in choosing the right magnitude of ϵ are the size of the solution, and the residuals after satisfying the inequalities. A change in ϵ changes the size of the null and range parts of the solution $\mathbf{b}$, and therefore also changes the residuals $\|\mathbf{Ab} - \Gamma\|$. A priori limits on the size of the solution and the residuals may help in determining the right ϵ for a given problem.

REFERENCES

Bretherton, F. P., R. E. Davis and C. B. Famdry, 1976: A technique for objective analysis and design of oceanographic experiments applied to MODE-73. *Deep Sea Res.*, **23**, 559–582.

Bryden, H. L., and H. Stommel, 1982: Origin of the Mediterranean outflow. *J. Mar. Res.*, **40**(Suppl.), 55–71.

El Gindy, A. A. H., 1982: Physical and dynamical structure of the Eastern Mediterranean. Ph.D. thesis, University of Alexandria, 206 pp.

Fiadeiro, M. E., and Veronis, G., 1984: Obtaining velocities from tracer distributions. *J. Phys. Oceanogr.*, **14**, 1734–1746.

Fu, Lee-Lueng, 1981: The general circulation and meridional heat transport of the subtropical south Atlantic determined by inverse methods. *J. Phys. Oceanogr.*, **11**, 1171–1193.

Hogg, N. G., 1987: A least-square fit of the advective diffusive equations to Levitus Atlas data. *J. Mar. Res.*, **45**(9), 347–375.

Lawson, C. L., and R. J. Hanson, 1974: *Solving Least Squares Problems,* Prentice-Hall, 340 pp.

Malanotte-Rizzoli, P., and A. Bergamasco, 1987. Modeling the general circulation of the Eastern Mediterranean Sea. Part I: the barotropic, wind driven circulation. Submitted.

May, W. P., 1982: Climatological flux estimates in the Mediterranean sea: Part I. Wind and wind stress. NORDA Rep 54.

Morcos, A. S., 1972: Sources of the Mediterranean Intermediate Water in the Levantine Sea. *Studies in Physical Oceanography,* Vol. 2, A. L. Gordon, Ed., Gordon and Breach, 185–206.

Olbers, D. J., M. Wenzel and J. Willebrand, 1985: The inference of North Atlantic circulation patterns from climatological hydrographic data. *Rev. Geophys.,* **23,** 313–356.

Özsoy, E. H., A. Latif and U. Unluata, 1981: On the formation of Levantine Intermediate Water in the Eastern Mediterranean. SACLANTCEN-SM-92. 45 pp.

Pedlosky, J., 1979: *Geophysical Fluid Dynamics.* Springer-Verlag, 624 pages.

POEM steering committee, 1985: UNESCO Reports in Marine Science, No. 35.

Redi, M. H., 1982: Oceanic isopycnal mixing by coordinate rotation. *J. Phys. Oceanogr.,* **12,** 1154–1158.

Robinson, A. R., A. Hecht, N. Pinardi, J. Bishop, W. G. Leslie, Z. Rosentroub, A. J. Mariano and S. Brenner, 1987: Small synoptic/mesoscale eddies: The energetic variability of the eastern Levantine basin. *Nature,* **327**(6118), 131–134.

Saunders, P. M., and Fofonoff, N. P., 1976: Conversion of pressure to depth in the ocean. *Deep-Sea Res.,* **23,** 109–111.

Schott, F., and H. Stommel, 1978: Beta spirals and absolute velocities in different oceans. *Deep-Sea Res.,* **25,** 961–1010.

Tziperman, E., 1988: Calculating the time-mean oceanic general circulation and mixing coefficients from hydrographic data. *J. Phys. Oceanogr.,* **18,** 519–525.

——, 1987: Mixing and general circulation dynamics: theory and observations. Ph.D. thesis. Woods Hole Oceanographic Institution/Massachusetts Institute of Technology Joint program in oceanography. 162 pp.

Wiggins, R. A., 1972: The general linear inverse problem: Implication to surface waves and free oscillations on earth structure. *Rev. Geophys.,* **10,** 251–285.

Wunsch, C., 1978: The general circulation of the North Atlantic west of 50°W determined from inverse methods. *Rev. Geophys.,* **16,** 583–620.

Wüst, G., 1960: On the vertical circulation of the Mediterranean Sea. *J. Geophys. Res.,* **66,** 3261–3271.